HHS Public Access

Author manuscript

Neurotox Res. Author manuscript; available in PMC 2021 October 01.

Published in final edited form as:

Neurotox Res. 2020 October ; 38(3): 751–764. doi:10.1007/s12640-020-00262-5.

The role of human LRRK2 in methylmercury-induced inhibition of microvesicle formation of cephalic neurons in *Caenorhabditis elegans*

Tao Ke[1], **Abel Santamaria**[2], **Joao BT Rocha**[3], **Alexey A. Tinkov**[4,5], **Rongzhu Lu**[6], **Aaron B Bowman**[7], **Michael Aschner**[1,5,*]

[1]Department of Molecular Pharmacology, Albert Einstein College of Medicine, Bronx, NY 10461, United States

[2]Laboratorio de Aminoácidos Excitadores, Instituto Nacional de Neurología y Neurocirugía, 14269, Mexico City, Mexico

[3]Department of Biochemistry and Molecular Biology, Federal University of Santa Maria, Santa Maria, RS, Brazil

[4]Yaroslavl State University, Sovetskaya St., 14, Yaroslavl 150000, Russia

[5]IM Sechenov First Moscow State Medical University, Sechenov University, Moscow, Russia.

[6]Department of Preventive Medicine and Public Health Laboratory Sciences, School of Medicine, Jiangsu University, Zhenjiang, Jiangsu 212013, China

[7]School of Health Sciences, Purdue University, West Lafayette, IN 47907-2051, United States

Abstract

In a previous study, we have shown that methylmercury (MeHg) exposure causes focal aggregation of intracellular transgenic mCherry protein in dendrites of cephalic (CEP) neurons in *Caenorhabditis elegans* (*C. elegans*). However, the underlying mechanism is unknown. We hypothesized that reduced cellular release of mCherry via extracellular vesicles by MeHg contributes to its accumulation and intracellular aggregation. Thus, we characterized vesicular structures in CEP dendrites, which were 1–3 μm in diameter and could readily bud off from the plasma membrane of the dendrites. Chronic treatment of *C. elegans* with MeHg (5 μM, 4–10 days) reduced the number of vesicles attached to CEP dendrites (attached vesicles) and vesicles unattached to CEP dendrites (unattached vesicles), as well as the presence of extracellular mCherry, supporting the hypothesis that release of mCherry by microvesicle formation is inhibited by MeHg. Leucine-rich repeat kinase 2 (LRRK2) has an important function in membrane biology.

*Corresponding author at: 1300 Morris Park Avenue, Forchheimer Building, Room 209, Bronx, NY 10461, Tel: 718.430.2317, Fax: 718.430.8922, michael.aschner@einstein.yu.edu.

Conflicts of interest

The authors declare no conflict of interest.

Further investigation showed that the effects of MeHg were modified by human *LRRK2*. In worms with the wild-type LRRK2, the vesicle numbers were significantly reduced by MeHg (0.5 and 5 μM). The effects of MeHg on the presence of extracellular mCherry and attached vesicles were modified by the human wild-type LRRK2. Independent of MeHg treatment, the G2019S mutant LRRK2 showed reduced number of unattached vesicles; however, the levels of extracellular mCherry were increased. Knockdown of *C. elegans irk-1,* the homolog of human *LRRK*2, reduced the number of attached vesicles, corroborating that LRRK2 plays an important role in the formation of microvesicles.

Keywords

methylmercury; Leucine-rich repeat kinase 2; CEP neuron; microvesicle

Introduction

In a previous study of *Caenorhabditis elegans* (*C. elegans*), we showed that transgenically expressed fluorescent protein mCherry was enriched in focal areas alongside the cephalic (CEP) dendrites after chronic exposure to methylmercury (MeHg), culminating in increased fluorescence signal with swelling puncta-like morphology. Yet background mCherry signals from the CEP dendrites were not increased by MeHg (Ke et al. 2020). A tentative explanation for these observations was that the enriched mCherry results from a failure of trans-cellular transfer or extracellular release of the dendritic localized mCherry (Melentijevic et al. 2017), where these molecules are sorted. However, the mechanisms of MeHg-induced damage to *C. elegans* dendrites have yet to be determined.

A major form of trans-cellular interchange of substances and organelles is the release and transfer of extracellular membrane vesicles (Kastelowitz and Yin 2014). Once fused with targeted recipient cell membranes, various cargos in the vesicles, including RNA, proteins, lipids, and even organelles, can be delivered to extracellular space, facilitating intercellular communications (Proia et al. 2008). An evolving concept of extracellular vesicles has been gaining attention, as this particular membrane structure has been involved in many important biological and pathogenic mechanisms. They are commonly found in biopsies of blood, cerebrospinal fluid, bile and saliva (Al-Nedawi et al. 2009; Kastelowitz and Yin 2014; Kosinski et al. 2005; Naegeli et al. 2017; Wang et al. 2014; Wehman et al. 2011). The extracellular membrane vesicles can be generally classified into two groups: exosomes and microvesicles (Al-Nedawi et al. 2009). The former refers to the extracellular vesicles that are released when multivesicular endosome fuses with plasma membrane, and they are of endosomal membrane origin and smaller in size (30–100 nm). Microvesicles are of plasma membrane origin and bigger in size (100–1000 nm), and are generated by outward budding and shedding from the plasma membrane (Kastelowitz and Yin 2014).

C. elegans is capable of secreting diverse vesicles for multiple regulatory purposes. By taking advantage of the long ventral nerve cord process, a well-characterized regulatory process is the transport and release of synaptic vesicles in the worm (Hall and Hedgecock 1991; Richmond et al. 1999). Besides the canonical synaptic vesicles for neurotransmission,

it shows that *C. elegans'* spermatozoa can protrude vesicles containing the signaling molecules that target oocytes to coordinate the maturation of the two germ lines (Kosinski et al. 2005). The budding of extracellular vesicles in *C. elegans* embryos are critical for embryonic morphogenesis (Wehman et al. 2011). The extracellular vesicles, released from the budding of the plasma membrane at the *C. elegans* male-specific cephalic male (CEM) ciliary base, act as a regional sensory cue by promoting male reversal and tail-chasing behavior (Wang et al. 2014). A multi-omic analysis of *C. elegans'* extracellular vesicles revealed that the marker of human extracellular vesicles (the tetraspanin: CD63) is a homolog of one of the most abundant proteins in the *C. elegans* extracellular vesicles (Russell et al. 2018), supporting that extracellular vesicles are conserved cellular process among species.

A recent study has shown that *C. elegans*' neuronal soma can excrete vesicles by membrane sprouting and fission (Melentijevic et al. 2017). The inclusion of vesicles encompasses disorganized proteins, damaged organelles, or toxic protein aggregates. It has been proposed that these vesicles represent a homeostatic mechanism to maintain optimal intracellular environment, as their numbers can be increased in response to a challenge with toxic proteins. Meanwhile, neurobehavioral analysis has revealed that vesicle formation by the soma represents an established mechanism in adult *C. elegans* for maintaining proper function of neurons. Although the significance of the discovery for brain diseases is speculative, earlier studies have shown that by secreting disease-causing toxic protein aggregates in externalized membrane vesicles, neurons propagate neurodegenerative pathology resembling Parkinson's disease (PD) (Emmanouilidou et al. 2010).

PD is an age-related neurodegenerative disease with progressive loss of dopaminergic (DAergic) neurons in the substantia nigra (SN) (Tolosa et al. 2020). Genetic studies have shown dozens of alleles that are causative to the disease, among which Leucine-rich repeat kinase 2 (LRRK2) mutations are the most common genetic cause of familial PD (Berwick et al. 2019; Zimprich et al. 2004). The LRRK2 protein has multiple domains including a kinase domain and a small-GTPase-like domain (Greggio et al. 2006). The G2019S mutation in the kinase domain is most frequently associated with PD (Luzon-Toro et al. 2007). Gain of function of the kinase domain associated with the G2019S mutation is closely related to the neurodegenerative pathogenesis of PD (Albanese et al. 2019; di Domenico et al. 2019). Although it remains largely unknown, the LRRK2 protein seems to function as a scaffold for large protein complexes juxtaposed with biological membranes, including autophagosome (Albanese et al. 2019; Roosen and Cookson 2016) and lysosomes, whose components are frequently found in extracellular vesicles and actively involved in plasma membrane repair and clearance of misfolded proteins (Reddy et al. 2001; Tsunemi et al. 2019).

In the *C. elegans* model of MeHg neurotoxicity, the morphology of CEP dendrites was characterized by a beading shape with focal aggregation of mCherry (Ke et al. 2020). In this model, we observed that CEP dendrites can form microvesicles and release mCherry to extracellular space. Herein, we further characterized the morphology of microvesicles in mCherry-labeled CEP dendrites, investigating the dynamics of the microvesicles in the nematode model. Furthermore, the effects of human LRRK2, the G2019S mutation, and the *C. elegans* homolog (*Irk-1*) on the formation of microvesicles were addressed.

Materials and methods

C. elegans strains and maintenance

C. elegans was cultured on OP50 seeded NGM plates in 20 °C incubator. The OH7193 [otIs181 III; him-8(e1489) IV], WLZ1 (wlzIs1 [snb-1p::Hsa-LRRK2 + lin15(+)]), WLZ3 (wlzIs3 [snb-1p::Hsa-LRRK2(G2019S) + lin15(+)])uIs60, and TU3311 ([unc-119p::YFP + unc-119p::sid-1]) strains were obtained from the Caenorhabditis Genetic Center (University of Minnesota). To cross WLZ1 with OH7193 and WLZ3 with OH7193, 6–10 young adult stage OH7193 male worms were mated with 4–6 late L4 stage hermaphrodites of WLZ1 and WLZ3, respectively. After 7–8 days, the F2 homozygotes of mCherry were genotyped for *LRRK2* with single worm PCR with primers reported earlier (Saha et al. 2009).

To synchronize worms, gravid stage worms were bleached, and worm debris and eggs were separated with 30% sucrose solution at 60 g for 7 min. After 16–18 h, newly hatched larvae stage 1 (L1) worms were treated in NGM medium (3 g NaCl, 2.5 g peptone, 975 ml H_2O, 1 ml cholesterol (5 mg/ml in ethanol), 1 ml nystatin, 1 ml 1 M $CaCl_2$, 1 ml 1 M $MgSO_4$, 25 ml pH 6 KPO_4), at 160 rpm with dead OP50 bacteria.

Measurement of attached vesicles and vesicles

To measure the diameters of attached vesicles and unattached vesicles, adult stage worms (6–20 for each group) treated with MeHg were imaged with confocal microscope (Leica SP8, Germany). As shown in Fig. 1, those attached to the dendrites are unreleased vesicles or attached vesicle, and those having a clear boundary with the dendrites are unattached vesicles. The diameter measurement of vesicles was made with Fiji software. Due to irregular shapes of attached vesicle, the diameter is defined as the distance from the center point of the basal part to the point at the apex of the budding head. To track the dynamics of the vesicular structures, worms were individually cultured in a single plate. Adult stage worms were paralyzed with 3 mM levamisole (Sigma, 1359302), and imaged at 0 h. After image acquisition, worms were carefully rehydrated with M9 buffer and placed back in the plates. After 4 h, the same worms were picked for imaging.

Counting of attached vesicles and vesicles

Worms treated with MeHg were paralyzed with 3 mM levamisole on 2% agarose pad poured on a glass slide. A thin small cover slide was placed on the agarose pad when the liquid was about to dry, yet sufficient quantity remained to soak the worms. Too much liquid causes refraction of the fluorescence light, while too little liquid harms the worms. Worms (10–30 per group) were picked onto the slide for manual counting of attached vesicles and unattached vesicles with epifluorescence microscope (Olympus BX41).

Feeding RNAi

The bacteria clone with RNAi plasmid targeting the sequence of T27C10.6 (*irk-1*, C. elegans homolog of human *LRRK2*) was obtained from the *C. elegans* RNAi collection (the Ahringer library). The RNAi bacteria were cultured on a special NGM plate with isopropylthio-β-galactoside (IPTG, 1 mM), and the ampicillin analog carbenicillin (100 μg/ml). Transformed bacteria with the vector plasmid L4440 served as control. The strain

TU3311 affords enhanced neuronal RNAi (Calixto et al. 2010). To cross TU3311 with OH7193, 6–10 young adult stage OH7193 male worms were mated with 4–6 late L4 stage hermaphrodites of TU3311. After 7–8 days, the F2 homozygotes of mCherry and GFP were selected under a fluorescence microscope. The TU3311*OH7193 strain was synchronized before feeding with the RNAi bacteria. The F1 adult stage worms of TU3311*OH7193 strain were treated with MeHg in NGM medium of RNAi bacteria with IPTG and carbenicillin.

We did a parallel experiment to knockdown neuronal GFP expression by RNAi feeding to the strain TU3311*OH7193; however, the GFP fluorescence was not significantly reduced in worms feeding with RNAi bacteria for at least 60 h. We reasoned that the GFP with a low turnover rate may not be an appropriate marker for the effect of RNAi, or alternatively the S65T variant of GFP which is used for construction of reporter strains has a relatively short time for maturation which makes it difficult to discriminate subtle difference in expression level (Boulin et al. 2006). Global level of *irk-1* mRNA is not an appropriate index for knockdown efficiency in the strain TU3311. To further assess the efficiency of RNAi knockdown to the gene *irk-1*, we analyzed the reference RNAi strain NL2099, resulting 95±3% reduction in the expression level of *irk-1* after 60-h feeding on RNAi bacteria lawn. Parental RNAi has a long-last knockdown effect to the offspring (Fire et al. 1998). To maximize the effect of RNAi, in our experiment, parental worms were fed with RNAi bacteria, and the next generation F1 adults on RNAi bacteria lawn were harvested.

Developmental stages of C. elegans

To calculate the percentage of *C. elegans* in various developmental stages, 80–100 worms per group were transferred to agar pads on glass slide, and evaluated under microscope (Olympus BX41) for the vulval developmental stage and typical dauer morphology, as described earlier (Apfeld and Kenyon 1998).

Statistical analysis

Numerical data with a normal distribution was analyzed with t-test, or one-way ANOVA and post hoc Tukey's multiple comparisons test (GraphPad 8.0.2). Categorical data were analyzed with Chi-square test followed by Chi-square partition method for multiple comparisons. When two experimental factors were analyzed, a two-way ANOVA test was performed. To explore the interactive effects of MeHg and Lrrk2, binary data was analyzed with logistic regression by SPSS 17.0 (Chicago, USA). $p \leq 0.05$ was considered to be statistically significant.

Result

In a previous study with the OH7193 strain, we observed that the fluorescence protein mCherry did not strictly reside within intracellular compartments of the tissues where the expression is driven by the neuron-type specific promoters. Thus, we posited that this transgenically expressed intracellular protein can be released to extracellular areas across the plasma membrane, promoting us to re-evaluate the morphology of DAergic neurons in the OH7193 strain.

In the head region, two pairs of CEP neurons have four dendrites extending to the mouth where the ciliary bases are located. The CEP dendrites rarely have branches or tangled structures. At the adult stage of OH7193 strain, we noted a sphere or oval shape membrane structure in the CEP dendrites (Fig. 1). The size and morphology of the membrane structures is consistent with their being extracellular microvesicles that originate from the dendritic membrane. To enable clarity in counting and assessing these vesicular structures, we defined those that are attached to the dendrites as “attached vesicles” (Fig. 1d and 1e), and those that have a clear boundary and are separated from the dendrite substructure as “unattached vesicles” (Fig. 1c). The size of attached vesicle and unattached vesicles had no significant difference, and most of them are in the range of 1 to 3 μm in diameter as measured by confocal microscopy (Fig. 1f).

Dynamic analysis spanning 4 h for the same CEP dendrites shows that the attached vesicles can shed off from the dendrite to become unattached vesicles (Fig. 2). Although some attached vesicles are able to progress to the unattached state, the membrane curvature in some of the early stage attached vesicles becomes flattened during this period (Fig. 2), suggesting that, in some cases, this process is reversible.

The size of attached vesicles was not significantly changed during the 4-hour observation (Fig. 3a, 3b and 3g). However, the unattached vesicles that shed off from the dendrites, became smaller or totally disappeared (Fig. 3c–3f). The size of unattached vesicles at 4 h was significantly reduced compared to those at 0 h (Fig. 3h).

To assess if MeHg exposure could modify this process, the OH7193 strain was treated in NGM medium for various time periods with 5 μM MeHg, the dose which was shown to significantly increase the rate of CEP mCherry puncta (Ke et al. 2020). Two-way ANOVA analysis showed that MeHg had a significant effect on the number of attached vesicles. Specifically, *post hoc* comparisons showed that MeHg treatment decreased the number of attached vesicles after 4, 8, or 10 days of exposure (Fig. 4). In the 6 d group, though the number of attached vesicles in MeHg-treated worms was lower than that in control worms, the difference did not reach to a significant level. In untreated worms, there was no significant change in the number of attached vesicles between the time points. In MeHg-treated worms, there was a significant decrease in the number of attached vesicles in the 10 d group compared to the 8 d group (Fig. 4).

The number of unattached vesicles was significantly decreased upon MeHg treatment. Two-way ANOVA analysis showed that MeHg had a significant decreasing effect (Fig. 5). The number of unattached vesicles was unchanged at the different time periods in untreated worms. In MeHg-treated worms, the number of unattached vesicles was significantly decreased in the day 4, day 6 and day 10 groups compared to control worms. In the 8 d group, the mean number of unattached vesicles in worms treated with MeHg was lower than that of the control group (without MeHg), but the difference failed to reach a statistically significant level ($p=0.082$).

To analyze the effect of human LRRK2 genes, the number of attached vesicles and unattached vesicles was counted in worms carrying the wild-type human LRRK2 gene

(LRRK2-wt) and the G2019S, a mutant LRRK2 gene (LRRK2-G2019S). Attached vesicle number was not significantly altered after a 10-d exposure to MeHg (Fig. 6a and 6b). However, the unattached vesicle number was significantly decreased after 10-d exposure of MeHg in the wild-type LRRK2 strain (LRRK2-wt, Fig. 6c). Notably, 0.05 μM MeHg decreased the number of unattached vesicles in the LRRK2-wt strain, and both higher doses (0.5 and 5 μM) had a significant effect (Fig. 6c). In contrast, in the LRRK2-G2019S strain, MeHg had no significant effects on the number of unattached vesicles (Fig. 6d).

The effects of MeHg and LRRK2 on the number of attached vesicles and unattached vesicles suggest that the extracellular level of mCherry might be affected. Next, the presence of mCherry in the peri-dendritic areas of the CEP neuron was investigated (Fig. 7). As shown in Figure 7, a worm is deemed positive if at least one side of the CEP dendrites has a type II or type III density of mCherry. This dichotomy method classifies the worms into the positive or negative phenotype based on whether there is a presence of extracellular mCherry. Similarly, a worm with at least one CEP attached vesicle or unattached vesicle is classified as positive in the analysis of vesicular structures.

Chi-Square analysis shows that 5 μM MeHg for 10 days decreased the percentage of the OH7193 worms (wt) with positive extracellular mCherry (Fig. 8a), attached vesicle (Fig. 8b), and unattached vesicle (Fig. 8c). However, in the strain harboring human wild-type LRRK2 (LRRK2-wt), the percentage of worms with positive extracellular mCherry was not changed with MeHg (Fig. 8a). It seems that the percentage of worms with attached vesicles in the strain towards an increase, but this does not reach a statistically significant level (Fig. 8b). However, the number of unattached vesicles was significantly decreased by MeHg (Fig. 8c).

In the LRRK2-G2019S strain, MeHg failed to alter the percentage of worms with positive extracellular mCherry, attached vesicle, or unattached vesicle (Fig. 8a, 8b and 8c). It is noteworthy that the percentage of worms with positive extracellular mCherry after MeHg treatment was significantly lower in the wt strain than that in stains with LRRK2-wt or LRRK2-G2019S (Fig. 8a). In worms absent of MeHg treatment, the percentage of positive extracellular mCherry was significantly lower in the wt strain than that in the LRRK-wt strain (Fig. 8a). The percentage of positive unattached vesicles in the LRRK2-G2019 strain without MeHg was lower than that in wt control worms; however, the difference did not reach to a significant level ($p=0.083$).

Binary logistic regression analysis shows that both MeHg and wild type LRRK2 had a significant effect on the percentage of extracellular mCherry (table 1). For attached vesicle, MeHg had a significant effect, and wild type LRRK2 had a significant interactive effect with MeHg. For unattached vesicle, MeHg had a significant effect, and the effect of the LRRK2-G2019S is near the significant level ($p=0.075$, table 1).

To investigate if the homolog of human LRRK2 in *C. elegans*, *irk-1*, is involved in the formation of the vesicular structures, a neuronal hypersensitive RNAi strain TU3311 was crossed with the OH7193 strain. The TU3311*OH7193 strain was fed with RNAi bacteria targeting *irk-1* for 3 days, after which the F1 adult stage worms fed with the RNAi bacteria

were harvested and treated for 24 h with MeHg in NGM medium. The two-way ANOVA indicated a significant interaction between MeHg x RNAi (knocking down of irk-1). In fact, in the worms fed with the RNAi vector L4440 control, MeHg tended to decrease the number of attached vesicles, but in the *irk-1* knockdown groups, MeHg tended to increase the number of attached vesicles in the relation to the control group (Fig. 9).

In the 10-day MeHg treatment experiment (Fig. 8), all the OH7193 strain worms were in the adult stage. For the OH7193*WLZ1 and OH7193*WLZ3 strains, some of the worms failed to reach the adult stage, so the development stage at day 10 was analyzed (Fig. 10). In the OH7193*WLZ1 strain (LRRK2-wt), the percentage of the younger L3 stage worms was significantly lower in worms treated with 5 μM MeHg compared to control worms (Fig. 10a). However, in the OH7193*WLZ3 strain (LRRK2-G2019S), MeHg failed to alter the distribution of L3 stage worms. For the two strains, some of worms were in dauer stage. MeHg had no effect on the percentage of dauer stage worms of LRRK2-wt or LRRK2-G2019S strain. The percentage of duaer stage worms was significantly higher in LRRK2-G2019S strain than LRRK2-wt strain. Binary logistic regression showed that the effect of MeHg on the percentage of L3 stage worms is significantly modified by LRRK2-G2019S. For dauer stage worms, LRRK2-G2019S had a significant effect, which was not modified by MeHg (Fig. 10c).

Discussion

The present study establishes that MeHg exposure inhibits the formation of vesicles in CEP dendrites and the effects are modified by human *LRRK2* gene. To our knowledge, this is the first study to characterize extracellular vesicles that are of CEP dendritic origin (Doroquez et al. 2014; Ward et al. 1975). As mCherry is released in the form of extracellular vesicles (Melentijevic et al. 2017), the failed formation of vesicle after MeHg exposure will gradually lead to the accumulation of mCherry and contribute to the large aggregates of mCherry (Ke et al. 2020), and possibly other toxic protein aggregates in CEP dendrites, eventually leading to dysfunction of CEP DAergic neurons.

The biological as well as pathological roles of vesicular structures have been delineated in studies with *C. elegans* and *in vitro* cell culture models (Emmanouilidou et al. 2010; Kosinski et al. 2005; Proia et al. 2008). In a study aimed to characterize the vesicular structure from neuronal soma in *C. elegans*, it was shown that the vesicular structure is a development-dependent neuronal protective strategy to rid the cells of damaged organelles and protein aggregates, which are associated with aging and proteotoxicity (Melentijevic et al. 2017). It has been demonstrated that protein aggregates in the cell can be spatially organized, with those insoluble aggregates being sorted into lysosome which components can be present in extracellular vesicles (Russell et al. 2018; Sontag et al. 2017; Tsunemi et al. 2019). Here, we show that the neurotoxicant MeHg is able to reduce the number of attached vesicles and unattached vesicles (Fig. 4 and 5), suggesting that the mCherry puncta observed in the early study might represent a failure of vesicle formation or release (Ke et al. 2020). Notably, worms with MeHg for 10 days had a significant lower number of attached vesicles than worms with MeHg for 8 days (Fig. 4), suggesting that the effect is modulated by intra-worm mercury which could be further increased in worms with 10-day MeHg

exposure compared with worms with 8-day MeHg exposure. Further studies on the toxicokinetics of MeHg in *C. elegans* are warranted to characterize the relationship between intra-worm level of mercury and toxic endpoints. In addition, MeHg is a pro-oxidant, which causes oxidative damage to cellular targets via inhibition of antioxidant selenoproteins (Farina et al. 2011). In the current model, MeHg could exert an inhibitory effect on the pathways of vesicular formation directly by oxidizing the cellular membrane system for genesis of extracellular vesicles or indirectly by increasing reactive oxygen species (ROS) (Bodega et al. 2019). On the other side, extracellular vesicles can scavenge ROS in the extracellular compartment, and instead of this beneficial effect they can also propagate oxidative stress by transferring oxidative molecules to target cells (Bodega et al. 2019). The role of extracellular vesicles in MeHg-induced oxidative stress can be further investigated in the *C. elegans* model by dynamic analysis of extracellular vesicles originated from dopaminergic neurons and site-specific analysis of oxidative stress. For example, chemical ROS-scavengers can be tested in the neuronal-cell specific ROS reporter strains for the better understanding of the potential role of ROS in the process.

The CEP attached vesicle and unattached vesicle numbers (Fig. 6 and 8), and extracellular mCherry (Fig. 8) were modified by human *LRRK2* in response to MeHg (table 1). The decline in the number of vesicular structures with MeHg is paralleled by lower rate of presence of extracellular mCherry in the OH7193 strain (Fig. 8). However, in the *LRRK2* transgenic worms, the rates of presence of extracellular mCherry were not changed with MeHg and were higher than those in the OH7193 strain (Fig. 8a). The extreme sensitivity of unattached vesicles other than attached vesicles or extracellular mCherry (Fig. 6 and 8) suggests that the fission process of vesicle formation is modulated by the human LRRK2, and this fits well with the notion that LRRK2 functions as a membrane scaffold protein to assembly a large protein complex to modulate membrane-mediated processes such as activity of chaperone-mediated autophagy (CMA) (Orenstein et al. 2013), synaptic vesicle recycling (Maas et al. 2017), and rate of exocytosis (Miklavc et al. 2014). It is intriguing that, even though the numbers of vesicular structure was not modified by the G2019S mutation, the rates of presence of extracellular mCherry were higher, suggesting that the basal activity of exportation or release other than the microvesicle pathway was triggered by the LRRK2 and the G2019S mutation (Fig. 8a).

The LRRK2 protein is a large protein (2527 amino acids) with multiple domains (GTPase domain, kinase domain, and WD40-like domain). The gain of function of the G2019S mutation increases the kinase activity, which is necessary for the pathogenic effects associated with PD (West 2017). Transfection of COS-7, HEK293, SH-SY5Y cell lines or primary cortical neurons with the G2019S LRRK2 construct induced an increased level of perinuclear inclusion body. An introduction of kinase-dead mutation reduced the level of inclusion body (Greggio et al. 2006), suggesting that the LRRK2 G2019S mutation is associated with increased activity of clearance of soluble protein aggregates destined for destruction by the perinuclear proteasome (Sontag et al. 2017). Astrocytes from PD patients carrying the G2019S mutation in the LRRK2 gene are capable of spreading aggregation-prone alpha-synuclein to co-cultured midbrain dopaminergic neurons from healthy individuals (di Domenico et al. 2019). We show that the G2019S mutation is associated with decreased basal levels of vesicles (Fig. 8), while the extracellular mCherry is increased,

corroborating that the G2019S LRRK2 increases the level of protein aggregation leading to the release of mCherry aggregates. Over-expression of wild type LRRK2 has a comparable level of extracellular mCherry to the G2019S LRRK2 (Fig. 8a), and this could result from the saturable activity of the kinase domain (Liu et al. 2016). In a model of manganese (Mn)-induced cytotoxicity, both pharmacological and genetic modulation of LRRK2 attenuated Mn-induced apoptosis in macrophages and microglia (Kim et al. 2019), and it is possible that the toxicity is also mediated by the compromised capacity of cellular protein homeostasis (Harischandra et al. 2019). As LRRK2 expression is maintained in cell bodies and processes in human postmortem midbrain tissue (Greggio et al. 2006), studies on the interactive effects of neurotoxicants and LRRK2 mutation will establish new preventive strategies for PD.

Irk-1, the *C. elegans* homolog of *LRRK2*, is required for polarized organization of synaptic vesicles by regulating protein sorting (Sakaguchi-Nakashima et al. 2007). IRK-1 works antagonistically with PINK-1 to modulate *C. elegans*' sensitivity to the mitochondria toxicant- paraquat (Samann et al. 2009). Coincidently, we show that knockdown of *irk-1* in neuronal tissue reduced the numbers of CEP attached vesicles (Fig. 9), corroborating that the endogenous IRK-1 is involved in the regulation of vesicle formation process, while over-expression of human LRRK2 seems to increase it (Fig. 8b). In addition, the kinase activity of human LRRK2 G2019S mutation has been shown to be involved in the damage to mitochondrial DNA (mtDNA) (Howlett et al. 2017), which could be the underlying mechanism for the increased percentage of dauer stage worms in the LRRK2-G2019S strain (Fig. 10) (Lee et al. 2003) and partly explain the reduced basal level of unattached vesicles in the strain (Fig. 6d).

In summary, by virtue of the transparency of the cells and mCherry labeled DAergic neurons in *C. elegans*, we have characterized the mCherry positive extracellular vesicles in CEP dendrites, which exhibited typical morphology of a microvesicle. Chronic treatment with MeHg reduced the numbers of attached vesicles and unattached vesicles, as well as the rate of extracellular mCherry, suggesting that the exportation of mCherry by microvesicle formation was inhibited by MeHg. Furthermore, the effects of MeHg were modified by expression of human *LRRK2*. Knockdown of C. elegan *irk-1,* the human *LRRK2* homolog, reduced the number of attached vesicle, corroborating that LRRK2 plays an important role in the formation of microvesicles. Although the failed release of mCherry is presumably a result of MeHg-induced decreased levels of vesicles, additional investigations on proteotoxicity models of *C. elegans* are warranted to establish a robust link between MeHg and the microvesicle pathway of protein homeostasis.

Acknowledgments

This work was supported by the National Institutes of Health to MA and ABB (NIEHS R01ES007331 and R01ES010563). The authors thank the Analytical Imaging Facility (AIF) at Albert Einstein College of Medicine, which is sponsored by NCI cancer center support grant P30CA013330 and Shared Instrumentation Grant (SIG) 1S10OD023591-01. Some strains were provided by the CGC, which is funded by NIH Office of Research Infrastructure Programs (P40 OD010440).

References

Al-Nedawi K, Meehan B, Rak J (2009) Microvesicles: messengers and mediators of tumor progression Cell Cycle 8:2014–2018 doi:10.4161/cc.8.13.8988 [PubMed: 19535896]

Albanese F, Novello S, Morari M (2019) Autophagy and LRRK2 in the Aging Brain Front Neurosci 13:1352 doi:10.3389/fnins.2019.01352

Apfeld J, Kenyon C (1998) Cell nonautonomy of C. elegans daf-2 function in the regulation of diapause and life span Cell 95:199–210 doi:10.1016/s0092-8674(00)81751-1 [PubMed: 9790527]

Berwick DC, Heaton GR, Azeggagh S, Harvey K (2019) LRRK2 Biology from structure to dysfunction: research progresses, but the themes remain the same Mol Neurodegener 14:49 doi:10.1186/s13024-019-0344-2 [PubMed: 31864390]

Bodega G, Alique M, Puebla L, Carracedo J, Ramirez RM (2019) Microvesicles: ROS scavengers and ROS producers Journal of extracellular vesicles 8:1626654 doi:10.1080/20013078.2019.1626654 [PubMed: 31258880]

Boulin T, Etchberger JF, Hobert O (2006) Reporter gene fusions WormBook:1–23 doi:10.1895/wormbook.1.106.1

Calixto A, Chelur D, Topalidou I, Chen X, Chalfie M (2010) Enhanced neuronal RNAi in C. elegans using SID-1 Nat Methods 7:554–559 doi:10.1038/nmeth.1463 [PubMed: 20512143]

di Domenico A, Carola G, Calatayud C, Pons-Espinal M, Munoz JP et al. (2019) Patient-Specific iPSC-Derived Astrocytes Contribute to Non-Cell-Autonomous Neurodegeneration in Parkinson's Disease Stem Cell Reports 12:213–229 doi:10.1016/j.stemcr.2018.12.011

Doroquez DB, Berciu C, Anderson JR, Sengupta P, Nicastro D (2014) A high-resolution morphological and ultrastructural map of anterior sensory cilia and glia in Caenorhabditis elegans Elife 3:e01948 doi:10.7554/eLife.01948 [PubMed: 24668170]

Emmanouilidou E, Melachroinou K, Roumeliotis T, Garbis SD, Ntzouni M et al. (2010) Cell-produced alpha-synuclein is secreted in a calcium-dependent manner by exosomes and impacts neuronal survival J Neurosci 30:6838–6851 doi:10.1523/jneurosci.5699-09.2010 [PubMed: 20484626]

Farina M, Aschner M, Rocha JB (2011) Oxidative stress in MeHg-induced neurotoxicity Toxicol Appl Pharmacol 256:405–417 doi:10.1016/j.taap.2011.05.001 [PubMed: 21601588]

Fire A, Xu S, Montgomery MK, Kostas SA, Driver SE et al. (1998) Potent and specific genetic interference by double-stranded RNA in Caenorhabditis elegans Nature 391:806–811 doi:10.1038/35888 [PubMed: 9486653]

Greggio E, Jain S, Kingsbury A, Bandopadhyay R, Lewis P et al. (2006) Kinase activity is required for the toxic effects of mutant LRRK2/dardarin Neurobiol Dis 23:329–341 doi:10.1016/j.nbd.2006.04.001 [PubMed: 16750377]

Hall DH, Hedgecock EM (1991) Kinesin-related gene unc-104 is required for axonal transport of synaptic vesicles in C. elegans Cell 65:837–847 doi:10.1016/0092-8674(91)90391-b [PubMed: 1710172]

Harischandra DS, Rokad D, Neal ML, Ghaisas S, Manne S et al. (2019) Manganese promotes the aggregation and prion-like cell-to-cell exosomal transmission of alpha-synuclein Science signaling 12 doi:10.1126/scisignal.aau4543

Howlett EH, Jensen N, Belmonte F, Zafar F, Hu X et al. (2017) LRRK2 G2019S-induced mitochondrial DNA damage is LRRK2 kinase dependent and inhibition restores mtDNA integrity in Parkinson's disease Human molecular genetics 26:4340–4351 doi:10.1093/hmg/ddx320 [PubMed: 28973664]

Kastelowitz N, Yin H (2014) Exosomes and microvesicles: identification and targeting by particle size and lipid chemical probes Chembiochem 15:923–928 doi:10.1002/cbic.201400043 [PubMed: 24740901]

Ke T, Tsatsakis A, Santamaria A, Antunes Soare FA, Tinkov AA et al. (2020) Chronic exposure to methylmercury induces puncta formation in cephalic dopaminergic neurons in Caenorhabditis elegans Neurotoxicology doi:10.1016/j.neuro.2020.01.003

Kim J, Pajarillo E, Rizor A, Son DS, Lee J et al. (2019) LRRK2 kinase plays a critical role in manganese-induced inflammation and apoptosis in microglia PLoS One 14:e0210248 doi:10.1371/journal.pone.0210248 [PubMed: 30645642]

Kosinski M, McDonald K, Schwartz J, Yamamoto I, Greenstein D (2005) C. elegans sperm bud vesicles to deliver a meiotic maturation signal to distant oocytes Development 132:3357–3369 doi:10.1242/dev.01916 [PubMed: 15975936]

Lee SS, Lee RY, Fraser AG, Kamath RS, Ahringer J et al. (2003) A systematic RNAi screen identifies a critical role for mitochondria in C. elegans longevity Nat Genet 33:40–48 doi:10.1038/ng1056 [PubMed: 12447374]

Liu Z, Mobley JA, DeLucas LJ, Kahn RA, West AB (2016) LRRK2 autophosphorylation enhances its GTPase activity FASEB J 30:336–347 doi:10.1096/fj.15-277095 [PubMed: 26396237]

Luzon-Toro B, Rubio de la Torre E, Delgado A, Perez-Tur J, Hilfiker S (2007) Mechanistic insight into the dominant mode of the Parkinson's disease-associated G2019S LRRK2 mutation Human molecular genetics 16:2031–2039 doi:10.1093/hmg/ddm151 [PubMed: 17584768]

Maas JW, Yang J, Edwards RH (2017) Endogenous Leucine-Rich Repeat Kinase 2 Slows Synaptic Vesicle Recycling in Striatal Neurons Front Synaptic Neurosci 9:5 doi:10.3389/fnsyn.2017.00005

Melentijevic I, Toth ML, Arnold ML, Guasp RJ, Harinath G et al. (2017) C. elegans neurons jettison protein aggregates and mitochondria under neurotoxic stress Nature 542:367–371 doi:10.1038/nature21362 [PubMed: 28178240]

Miklavc P, Ehinger K, Thompson KE, Hobi N, Shimshek DR et al. (2014) Surfactant secretion in LRRK2 knock-out rats: changes in lamellar body morphology and rate of exocytosis PLoS One 9:e84926 doi:10.1371/journal.pone.0084926 [PubMed: 24465451]

Naegeli KM, Hastie E, Garde A, Wang Z, Keeley DP et al. (2017) Cell Invasion In Vivo via Rapid Exocytosis of a Transient Lysosome-Derived Membrane Domain Dev Cell 43:403–417 e410 doi:10.1016/j.devcel.2017.10.024

Orenstein SJ, Kuo SH, Tasset I, Arias E, Koga H et al. (2013) Interplay of LRRK2 with chaperone-mediated autophagy Nat Neurosci 16:394–406 doi:10.1038/nn.3350 [PubMed: 23455607]

Proia P, Schiera G, Mineo M, Ingrassia AM, Santoro G et al. (2008) Astrocytes shed extracellular vesicles that contain fibroblast growth factor-2 and vascular endothelial growth factor International journal of molecular medicine 21:63–67 [PubMed: 18097617]

Reddy A, Caler EV, Andrews NW (2001) Plasma membrane repair is mediated by Ca(2+)-regulated exocytosis of lysosomes Cell 106:157–169 doi:10.1016/s0092-8674(01)00421-4 [PubMed: 11511344]

Richmond JE, Davis WS, Jorgensen EM (1999) UNC-13 is required for synaptic vesicle fusion in C. elegans Nat Neurosci 2:959–964 doi:10.1038/14755 [PubMed: 10526333]

Roosen DA, Cookson MR (2016) LRRK2 at the interface of autophagosomes, endosomes and lysosomes Mol Neurodegener 11:73 doi:10.1186/s13024-016-0140-1 [PubMed: 27927216]

Russell JC, Merrihew GE, Robbins JE, Postupna N, Kim T-K et al. (2018) Isolation and characterization of extracellular vesicles from Caenorhabditis elegans for multi-omic analysis:476226 doi:10.1101/476226 %J bioRxiv

Saha S, Guillily MD, Ferree A, Lanceta J, Chan D et al. (2009) LRRK2 modulates vulnerability to mitochondrial dysfunction in Caenorhabditis elegans J Neurosci 29:9210–9218 doi:10.1523/JNEUROSCI.2281-09.2009 [PubMed: 19625511]

Sakaguchi-Nakashima A, Meir JY, Jin Y, Matsumoto K, Hisamoto N (2007) LRK-1, a C. elegans PARK8-related kinase, regulates axonal-dendritic polarity of SV proteins Current biology : CB 17:592–598 doi:10.1016/j.cub.2007.01.074 [PubMed: 17346966]

Samann J, Hegermann J, von Gromoff E, Eimer S, Baumeister R et al. (2009) Caenorhabditits elegans LRK-1 and PINK-1 act antagonistically in stress response and neurite outgrowth J Biol Chem 284:16482–16491 doi:10.1074/jbc.M808255200 [PubMed: 19251702]

Sontag EM, Samant RS, Frydman J (2017) Mechanisms and Functions of Spatial Protein Quality Control Annu Rev Biochem 86:97–122 doi:10.1146/annurev-biochem-060815-014616 [PubMed: 28489421]

Tolosa E, Vila M, Klein C, Rascol O (2020) LRRK2 in Parkinson disease: challenges of clinical trials Nat Rev Neurol 16:97–107 doi:10.1038/s41582-019-0301-2 [PubMed: 31980808]

Tsunemi T, Perez-Rosello T, Ishiguro Y, Yoroisaka A, Jeon S et al. (2019) Increased Lysosomal Exocytosis Induced by Lysosomal Ca(2+) Channel Agonists Protects Human Dopaminergic

Neurons from alpha-Synuclein Toxicity J Neurosci 39:5760–5772 doi:10.1523/jneurosci.3085-18.2019 [PubMed: 31097622]

Wang J, Silva M, Haas LA, Morsci NS, Nguyen KC et al. (2014) C. elegans ciliated sensory neurons release extracellular vesicles that function in animal communication Current biology : CB 24:519–525 doi:10.1016/j.cub.2014.01.002 [PubMed: 24530063]

Ward S, Thomson N, White JG, Brenner S (1975) Electron microscopical reconstruction of the anterior sensory anatomy of the nematode Caenorhabditis elegans.?2UU J Comp Neurol 160:313–337 doi:10.1002/cne.901600305 [PubMed: 1112927]

Wehman AM, Poggioli C, Schweinsberg P, Grant BD, Nance J (2011) The P4-ATPase TAT-5 inhibits the budding of extracellular vesicles in C. elegans embryos Current biology : CB 21:1951–1959 doi:10.1016/j.cub.2011.10.040 [PubMed: 22100064]

West AB (2017) Achieving neuroprotection with LRRK2 kinase inhibitors in Parkinson disease Exp Neurol 298:236–245 doi:10.1016/j.expneurol.2017.07.019 [PubMed: 28764903]

Zimprich A, Biskup S, Leitner P, Lichtner P, Farrer M et al. (2004) Mutations in LRRK2 cause autosomal-dominant parkinsonism with pleomorphic pathology Neuron 44:601–607 doi:10.1016/j.neuron.2004.11.005 [PubMed: 15541309]

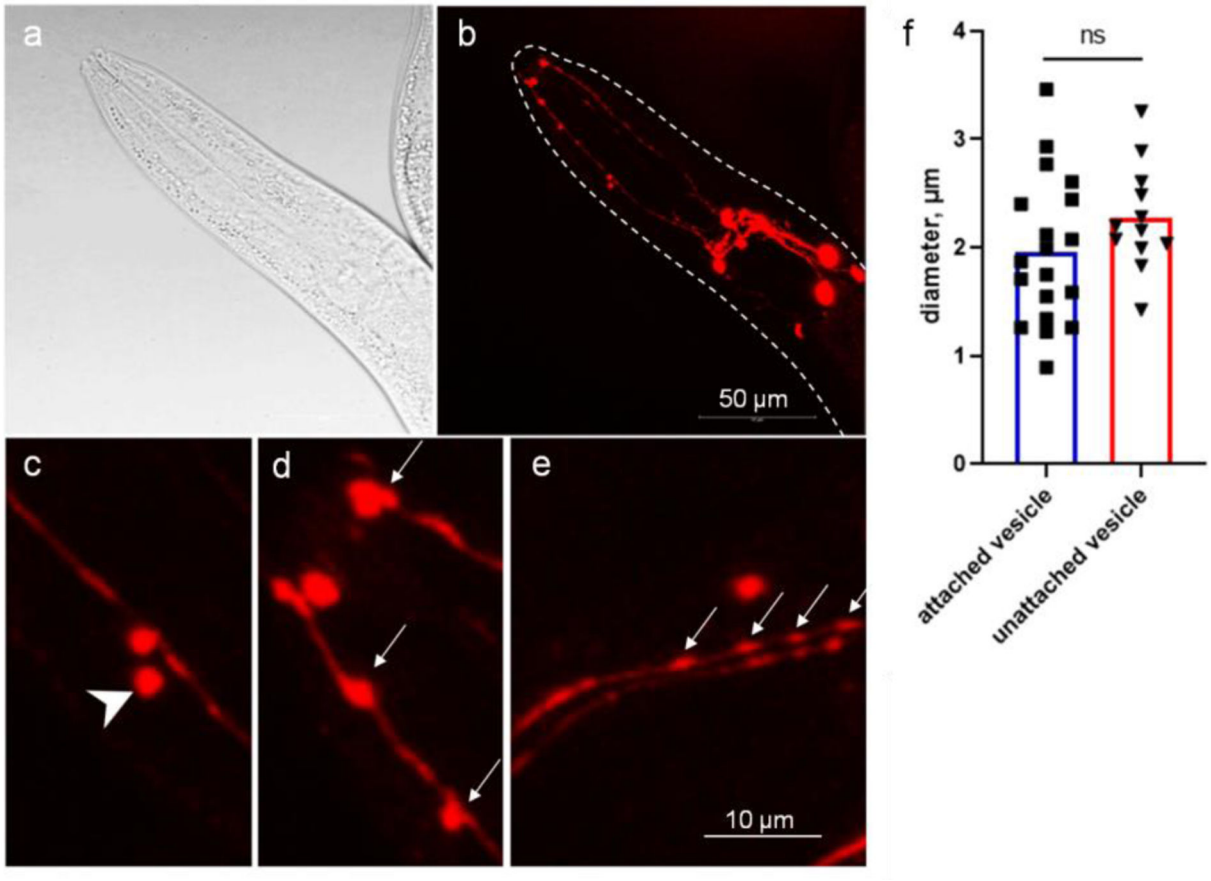

Figure 1.

C. elegans CEP dendrites produce microvesicles. Images of adult stage of the OH7193 strain were acquired by Leica SP8 confocal microscope. a, bright field image of the head region. b, corresponding image of DAergic neurons in the head region. c, unattached vesicle shed from the CEP dendrite. d and e, attached vesicle on the CEP dendrites. Arrow head shows unattached vesicle; arrows show attached vesicle. f, diameters of the vesicular structures in the CEP dendrites. t-test.

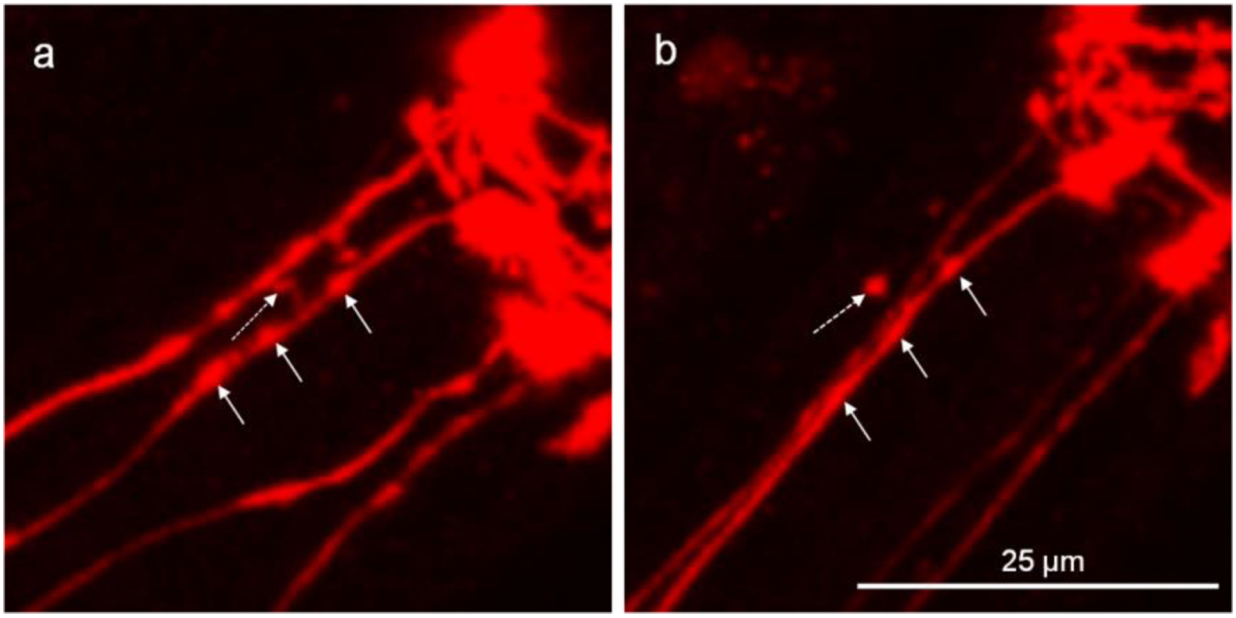

Figure 2.

Attached vesicles shed off the CEP dendrite to become unattached vesicles. The head region of DAergic neurons was imaged to show the four parallel CEP dendrites. a, the dotted-line arrow shows the attached vesicle which is linked to the dendrite with a thin tubular structure, and the other straight-line arrows show the areas that are likely to form attached vesicles. b, of the same worm from “a” after a 4-h period, shows the attached vesicle shed off from the dendrite, while the areas that are likely to form attached vesicles become flattened.

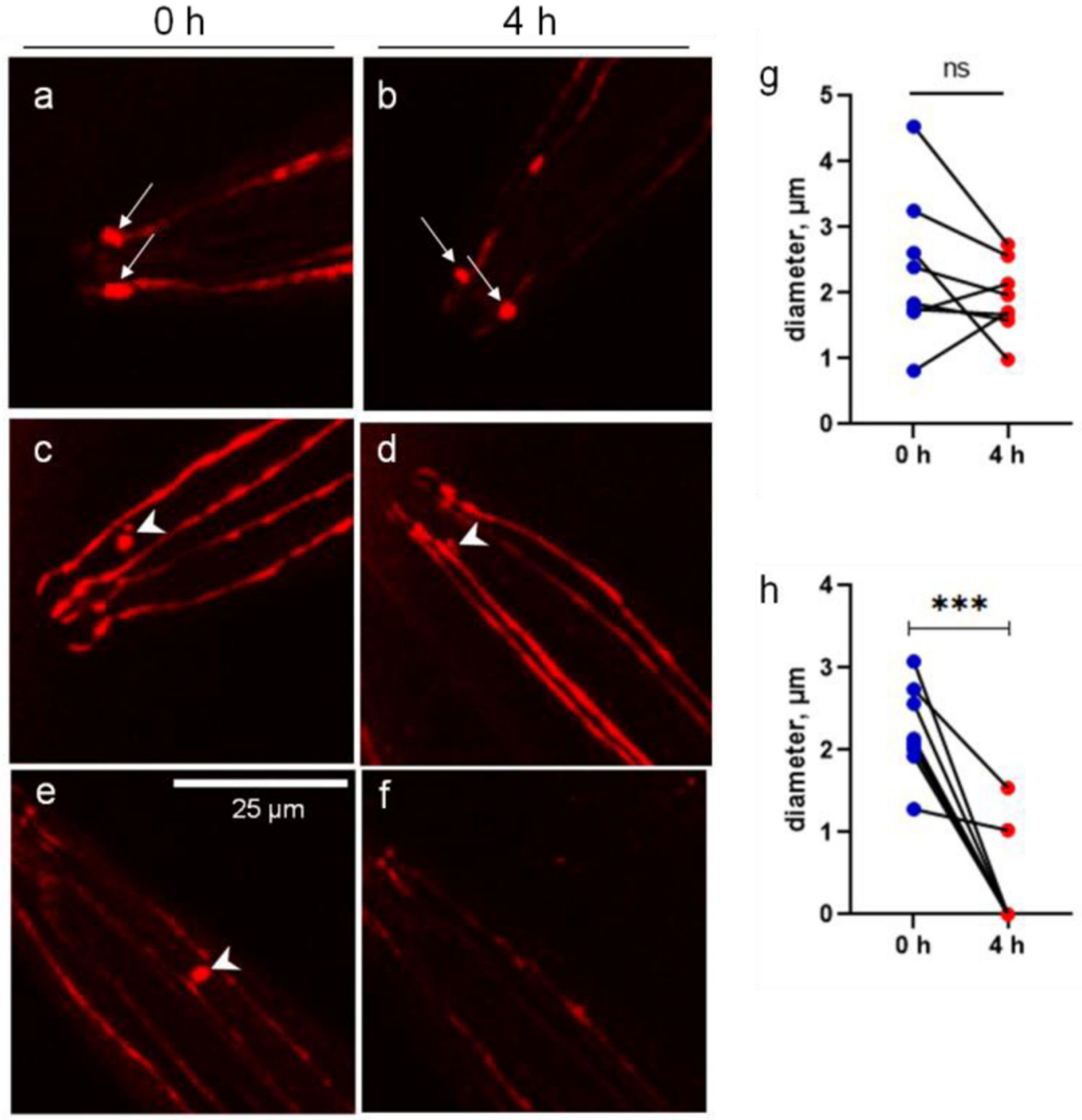

Figure 3.

The CEP vesicles are dissolved during a 4-h period. The images of single-worm tracking show the dynamics of attached vesicles (arrow) and unattached vesicles (arrow head). a and b, show two attached vesicles at the CEP ciliary bases in the proximity of mouth area. c and d, show the unattached vesicle becomes much smaller after a 4-h period. e and f, show the unattached vesicle becomes invisible after a 4-h period. g, diameters of attached vesicles at 0 and 4 h. h, diameters of unattached vesicles at 0 and 4 h. ***$p<0.001$, paired t-test.

a

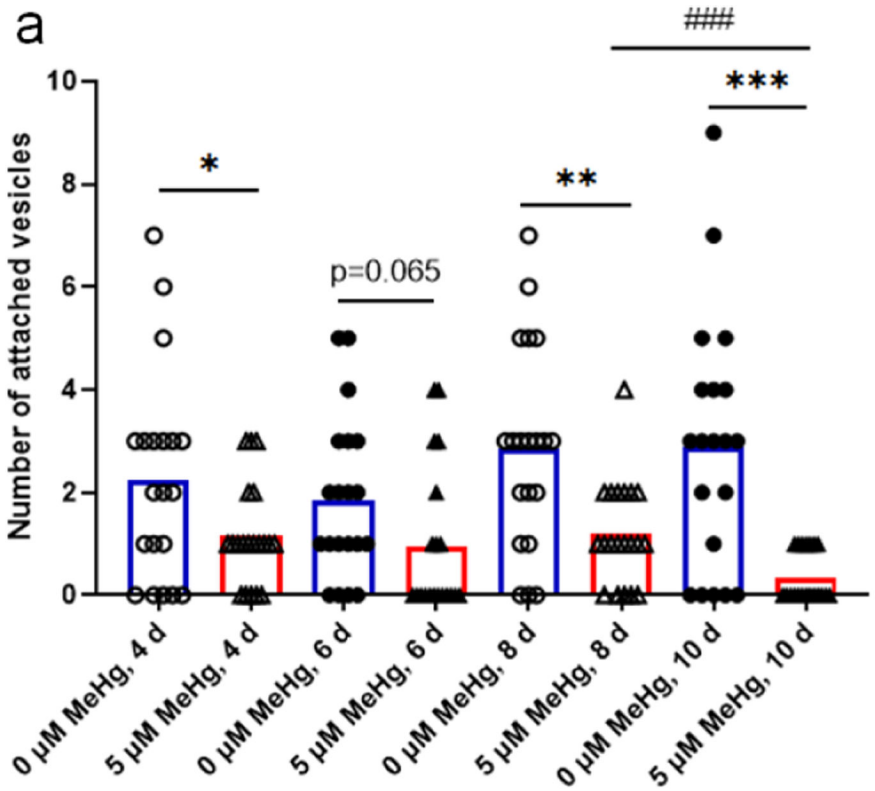

b

	SS	DF	F	P value
Time	8.03	3	1.03	P=0.380
MeHg	96.10	1	37.08	P<0.0001
Interaction	16.35	3	2.10	0.102

Figure 4.

CEP attached vesicle numbers are decreased with MeHg exposure. The number of attached vesicles on the four CEP dendrites of the OH7193 strain dosed with MeHg for different periods was counted with epi-fluorescence microscope. a, MeHg exposure reduced the number of attached vesicles. b, two-way ANOVA analysis of the effects of time and MeHg exposure on the number of attached vesicles. The results were derived from 15–20 worms for each group. SS, sum of squares; DF, degree of freedom; F, F ratio.

a

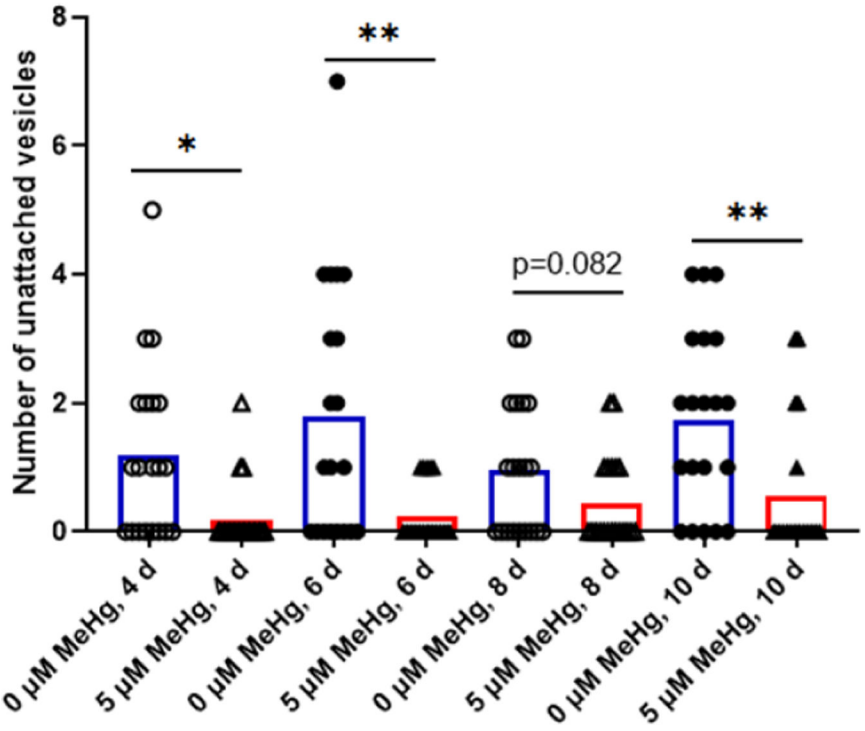

b

	SS	DF	F	P value
Time	6.32	3	1.53	P=0.210
MeHg	45.16	1	32.69	P<0.0001
Interaction	5.77	3	1.39	0.247

Figure 5.

The CEP unattached vesicle numbers are decreased with MeHg exposure. The number of unattached vesicles in the four CEP dendrites of the OH7193 strain dosed with MeHg for different periods was counted with epi-fluorescence microscope. a, MeHg exposure decreased the number of unattached vesicles. b, two-way ANOVA analysis of the effects of time and MeHg exposure on the number of unattached vesicles. The results were derived from 15–20 worms for each group. SS, sum of squares; DF, degree of freedom; F, F ratio.

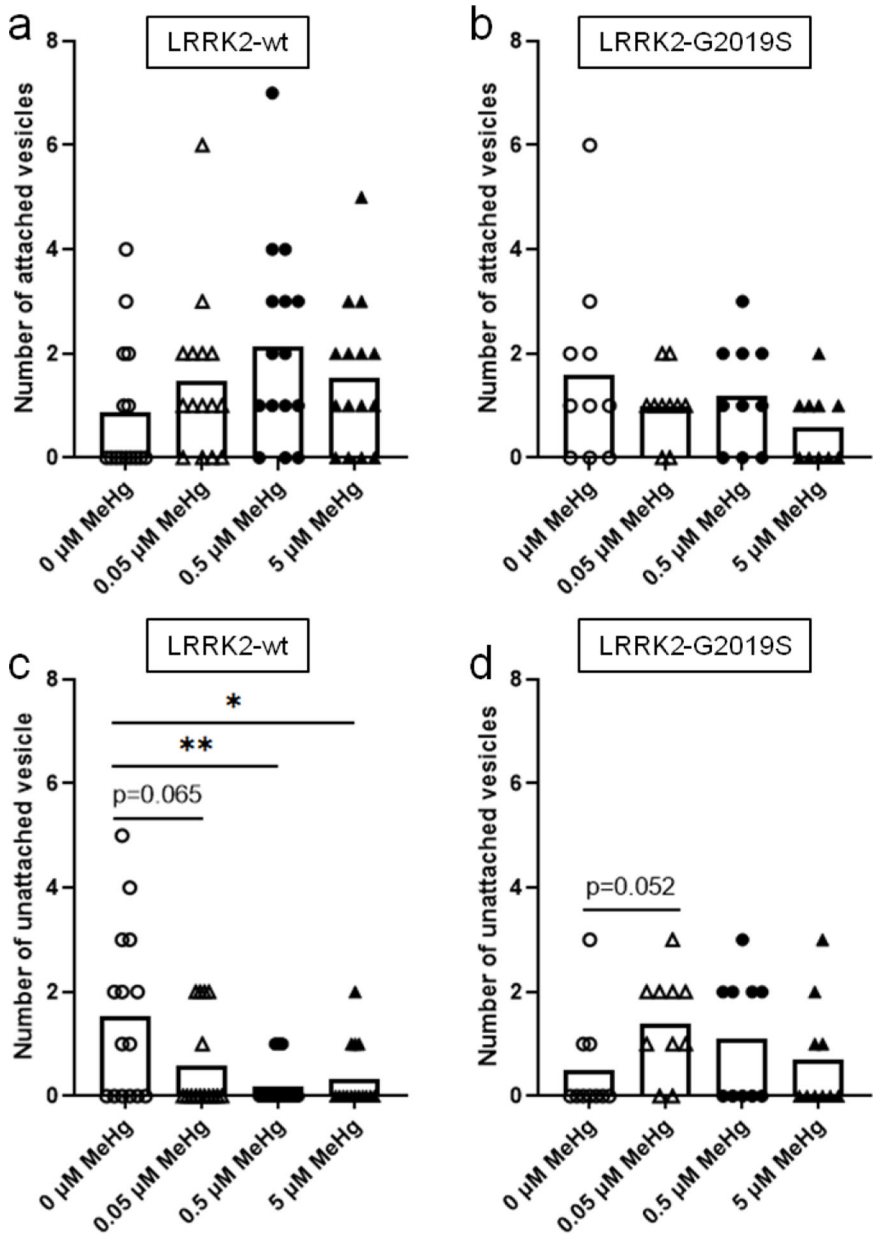

Figure 6.

The number of CEP sourced extracellular vesicles is altered by expression of human LRRK2 and MeHg exposure. The OH7193 strain was crossed with the WLZ1 (LRRK2-wt) and WLZ3 strain (LRRK2-G2019S) respectively to observe the effect of human LRRK2 genes on the number of vesicular structures. a and b, the numbers of attached vesicles from the CEP dendrites in the OH7193*WLZ1 and OH7193*WLZ3 strains dosed with graded concentrations of MeHg. c and d, the numbers of unattached vesicles from the CEP dendrites in the OH7193*WLZ1 and OH7193*WLZ3 strains treated with MeHg. Comparisons were made by one-way ANOVA and Tukey's multiple comparisons test. *P<.05, **P<.01, and ***P<.001.

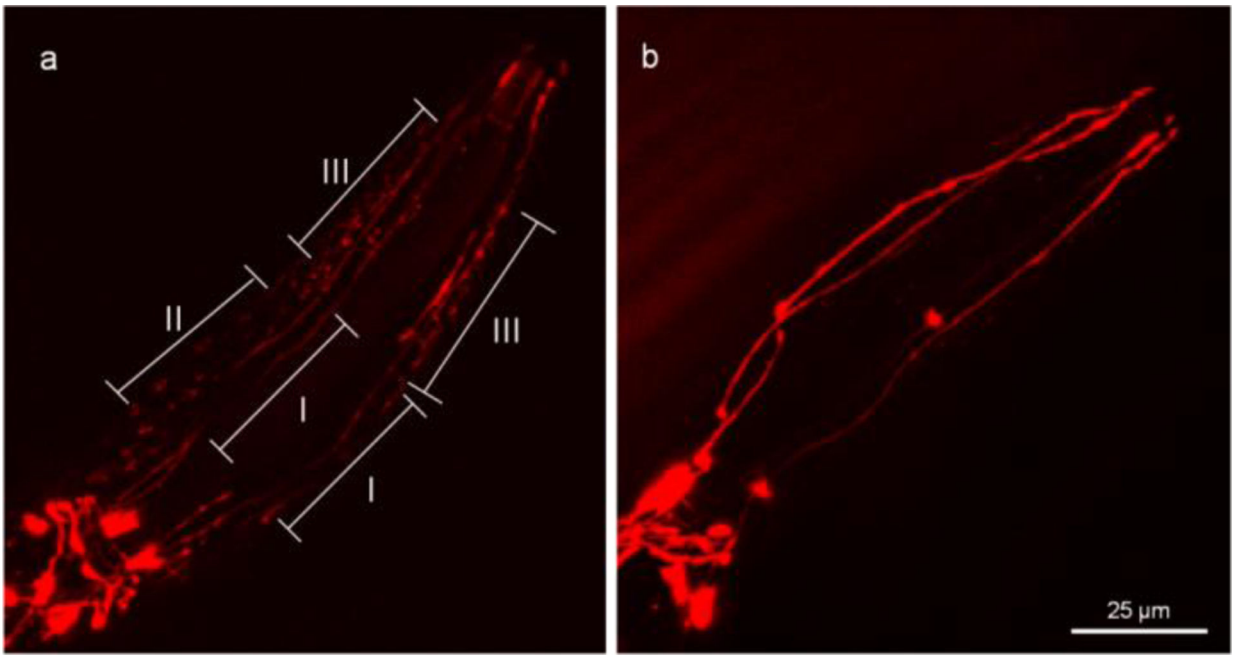

Figure 7.

mCherry protein is present outside the CEP dendrites. The head region of the OH7193 strain was imaged to show the extracellular presence of mCherry. The presence of mCherry in vicinity of CEP dendrites is classified into three types according to density of mCherry. Both the type II and III are positive, but the type I is negative. A worm is positive if at least one side of CEP dendrites has a type II or type III density of mCherry. a, a worm with positive presence of mCherry in the peri-areas around the CEP dendrites. b, a worm with negative presence of mCherry in the peri-areas around the CEP dendrites.

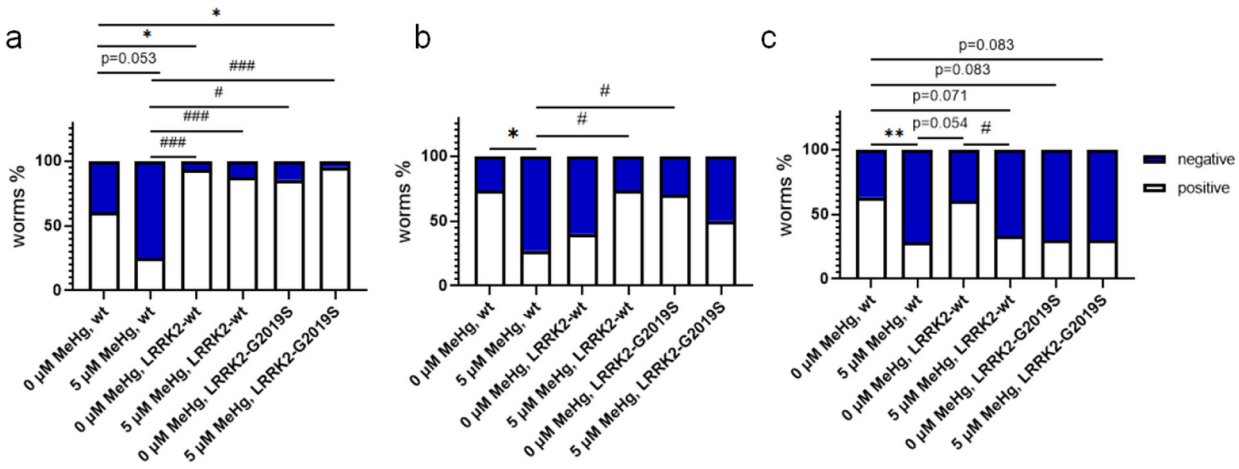

Figure 8.

Repression of mCherry transcytosis and extracellular vesicular formation by MeHg is modified by LRRK2. The OH7193 (wt), wild type LRRK2 transgenic (OH7193*WLZ1, LRRK2-wt), and mutant LRRK2 transgenic (OH7193*WLZ3, LRRK2-G2019S) worms were scored for the presence of mCherry outside of CEP dendrites (a), attached vesicles (b), and unattached vesicles from CEP dendrites (c). 10–30 worms for each group were scored. Part of the data here is the same of those from figures 4–6. Analysis was made with Chi-square test. *P<.05, $^{\#}$P<.05, **P<.01, and $^{\#\#\#}$P<.001.

a

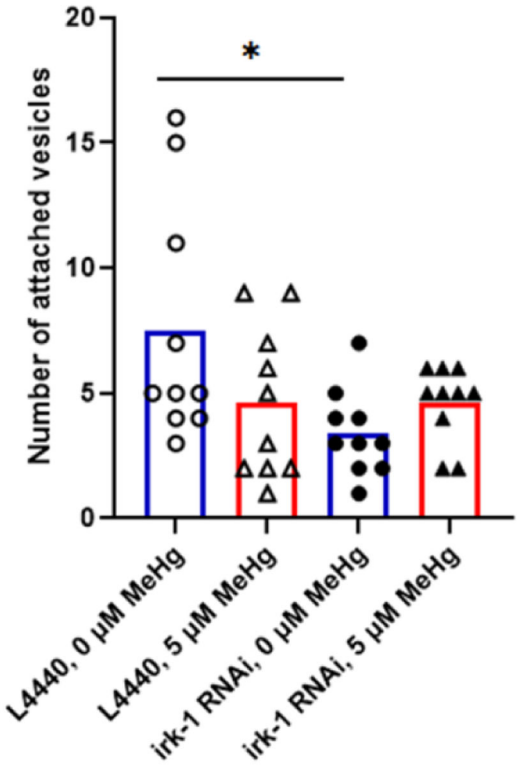

b

	SS	DF	F	P value
RNAi	42.03	1	4.53	0.040
MeHg	7.23	1	0.78	0.383
Interaction	42.03	1	4.53	0.040
Residual	333.70	36		

Figure 9.

Know-down *irk-1* in neurons reduces the number of the CEP attached vesicle in adult *C. elegans*. The OH7193 strain was crossed with the TU3311 strain to generate a hypersensitive neuronal RNAi strain with DAergic expression of mCherry (OH7193*TU3311). The adult stage F1 generation of the OH7193*TU3311 fed with RNAi bacteria were treated with MeHg for 24 h. a, number of the CEP attached vesicles in the OH7193*TU3311 strain treated with MeHg. b, two-ANOVA analysis indicated a significant interaction between the effect of RNAi and MeHg on the number of attached vesicles. SS, sum of squares; DF, degree of freedom; F, F ratio. *P<.05.

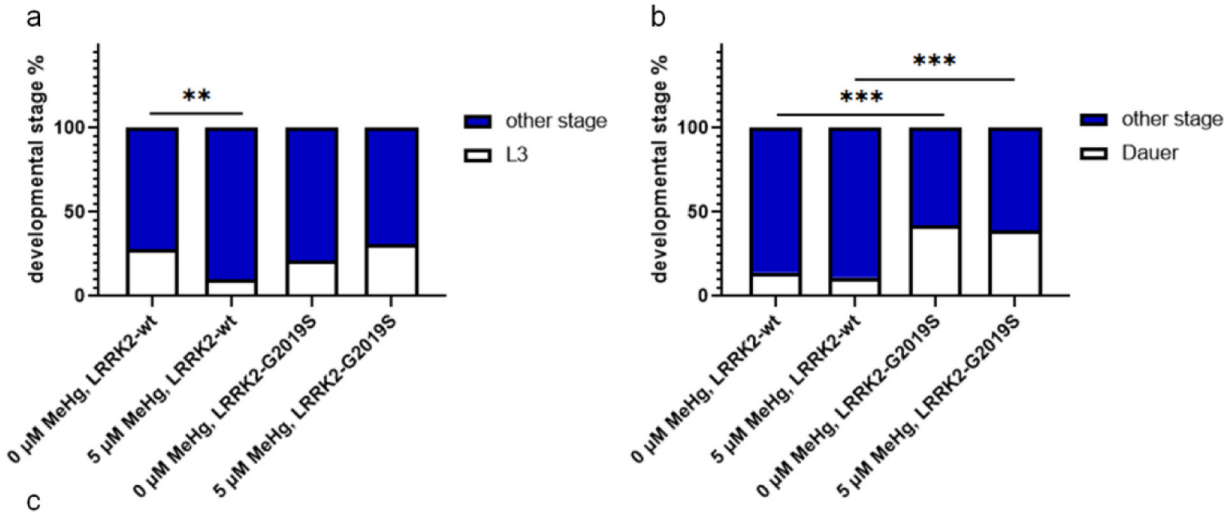

c

Rate%	factors	Wald	df	P value
L3	MeHg	13.033	1	<0.001
	LRRK2-G2019S	2.130	1	0.144
	Interaction (MeHg, LRRK2-G2019S)	19.008	1	<0.001
Dauer	MeHg	0.370	1	0.543
	LRRK2, G2019S	27.806	1	<0.001
	Interaction (MeHg, LRRK2-G2019S)	0.197	1	0.657

Figure 10.

The association of developmental stage with MeHg is dependent on the genotypes of LRRK2. The developmental stage of the OH7193*WLZ1 (LRRK2-wt) and OH7103*WLZ3 (LRRK2-G2019S) strains were analyzed after treatment with MeHg for 10 days. a, MeHg treatment (5 μM) decreases the percentage of L3 stage worms in the OH7193*WLZ1 (LRRK2-wt) strain. b, no significant effects of MeHg on the percentage of dauer stage worms. Analysis was made with Chi-square test. **P<.01, and ***P<0.001. c. binary logistic regression for the effects of MeHg and LRRK2-G2019S on the percentage of L3, or dauer stage worms.

Table 1.

The effects of MeHg and LRRK2 on the rate of extrcellular mCherry, attached vesicle and vesicle.

%	Factors*	Wald	df	P value
extracellular mCherry	MeHg	4.763	1	0.029
	LRRK2-wt	3.898	1	0.048
	LRRK2-G2019S	0.285	1	0.593
	Interaction (MeHq, LRRK2)	0.256	2	0.880
Attached vesicle	MeHg	6.004	1	0.014
	LRRK2-wt	3.246	1	0.072
	LRRK2-G2019S	0.033	1	0.856
	Interaction (MeHg, LRRK2)	9.429	2	0.009
	Interaction (MeHg, LRRK2-wt)	9.101	1	0.003
	Interaction (MeHq, LRRK2-G2019S)	0.888	1	0.346
Unattached vesicle	MeHg	8.772	1	0.003
	LRRK2-wt	0.029	1	0.865
	LRRK2-G2019S	3.165	1	0.075
	Interaction (MeHg, LRRK2)	1.801	2	0.406

*, analysis was made with binary logistic regression.